Modelling IP effects in airborne time domain electromagnetics

Dave Marchant*
Computational Geosciences
Vancouver, BC, Canada
dave@compgeoinc.com

Seogi Kang
University of British Columbia
Vancouver, BC, Canada
skang09@gmail.com

Mike McMillian
Computational Geosciences
Vancouver, BC, Canada
mike@compgeoinc.com

Eldad Haber
University of British Columbia
Vancouver, BC, Canada
eldadhaber@gmail.com

*presenting author asterisked

SUMMARY

The presence of chargeable materials can significantly impact the data in electromagnetic (EM) surveys. This affected data has traditionally been treated as noise that must be removed prior to interpretation or inversion. The ability to extract induced polarization (IP) information from an airborne platform would be a valuable tool in the mineral exploration industry, and thus the pursuit of this ability has recently led to significant interest in the interpretation of IP effects in airborne data. A variety of interpretation methodologies have been proposed to aid in the identification and extraction of information from time domain EM data containing IP effects. Any interpretation scheme needs to be thoroughly tested on realistic synthetic examples so that the strengths and weaknesses of the method are well understood.

In this work, we present a methodology for accurately and efficiently simulating the response of a time domain EM experiment by modelling the convolution that occurs in Ohm's Law in the presence of a frequency dependent conductivity. This method is free of any assumptions about the dimensionality or frequency dependence of the chargeable material and can be used to simulate the response of any time domain system.

Key words: Electromagnetics, Induced polarization, Forward modelling

INTRODUCTION

The economic importance of chargeable materials has generated a large body of work focusing on the forward modelling of their electromagnetic response. The ability to simulate these responses provides an invaluable tool
when trying to understand and interpret observations. Simulating the electromagnetic response of chargeable materials in the frequency domain is, in principle, straight forward. However, modelling the response of a frequency dependent conductivity in the time domain is computationally challenging.

Early work on this problem focused primarily on modelling the response of geometrically simple polarizable bodies. This is accomplished by either transforming results from the frequency-domain to the time-domain (Bhattacharyya, 1964; Flis et al., 1989; Hohmann and Newman, 1990; Lee, 1975, 1981; Lee and Thomas, 1992; Lewis and Lee, 1984; Morrison et al., 1969; Rathor, 1978; Wait and Debroux, 1984), or by treating the time domain convolution directly (Smith et al., 1988). Zaslavsky and Druskin (2010) and Zaslavsky et al. (2011) developed a modelling technique based on the rational Krylov subspace projection approach that can model the response of a three-dimensional distribution of chargeable material. However, their technique still required a frequency-to-time domain transformation.

Techniques making use of frequency-to-time domain transformations can easily incorporate frequency dependent conductivities, but are only efficient when modelling sources containing a small number of frequencies. Accurately modelling sources containing a broad band of frequency content, such as the square waves commonly used in time domain electromagnetic or induced polarization experiments, requires the solution of Maxwell's equations for a large number of frequencies. For example, Newman et al. (1986) and Flis et al. (1989) reported requiring between 20 and 50 frequencies to accurately model a step-off response. If iterative methods are employed, the response at each frequency can be calculated in parallel. This makes frequency domain methods efficient at solving problems with a limited number of sources, however, they quickly become computationally limiting as the number of sources grows (da Silva et al., 2012; Streich, 2009).

The problem can also be considered directly in the time domain. A few different approaches have been taken to make this possible. Two recent methods include limiting the frequency dependence of the media to one that can be approximated with a Pade approximation (Marchant et al., 2014) or weighted sum of Debye models (Commer et al., 2017). While these techniques overcome the problems of working in the frequency domain, they limit the range of frequency dependencies that can be modelled.

In this work, a technique for modelling the electromagnetic response of a three-dimensional distribution of chargeable material is developed. The technique models the convolutionary nature of Ohm's law directly, avoiding the need for frequency to time domain transformations. The technique is tested by comparing results to analytic half-space responses and is then demonstrated for a three-dimensional example.

Theory

Multiplication in the frequency domain results in a convolution when transformed to the time domain. For dispersive conductivities, Ohm's law in the time domain is therefore given by the following convolution,

$$\vec{j}(t) = \int_{-\infty}^{\infty} \sigma(t-\tau)\vec{e}(\tau)d\tau \tag{1}$$

where $\sigma(t)$ is the impulse response of the frequency dependant conductivity. Due to the causal nature of the system, $\sigma(t)$ must have the form

$$\sigma(t) = \begin{cases} 0, & t < 0 \\ \sigma_{\infty}, & t = 0 \\ -\hat{\sigma}(t), & t > 0 \end{cases} \tag{2}$$

Combining these two equations with Ampere's and Faraday's Law gives the system of equations

$$\vec{\nabla} \times \vec{e} + \frac{\partial \vec{b}}{\partial t} = 0$$
$$\vec{\nabla} \times \frac{1}{\mu}\vec{b} - \vec{j} = \vec{J_s} \tag{3}$$
$$\vec{j}(t) = \sigma_{\infty}\vec{e}(t) - \int_{0}^{t} \hat{\sigma}(t-\tau)\vec{e}(\tau)d\tau$$

The solution of this system will provide the electromagnetic response of a chargeable earth.

METHOD

Discretization of Ohm's law in time

In this section, we derive an approach to numerically approximate the convolutionary form of Ohm's law for materials exhibiting a Cole-Cole frequency dependence. The goal is to approximate Equation 4.4 in terms of electric fields given at a set of discrete times. In this way, a version of Ohm's law can then be included in an explicit time-stepping electromagnetic forward modelling routine.

The time axis is divided into N+1 discrete points $[t^{(0)}, t^{(1)}, \dots, t^{(N)}]$ with

$$\delta t^{(n)} = t^{(n)} - t^{(n-1)} \tag{4}$$

Splitting the integral in Equation 3 into time steps gives

$$\vec{j}(t) = \sigma_{\infty}\vec{e}(t) - \int_{0}^{t^{(1)}} \hat{\sigma}(t^{(n)} - \tau)\vec{e}(\tau)d\tau - \cdots - \int_{t^{(n-1)}}^{t^{(n)}} \hat{\sigma}(t^{(n)} - \tau)\vec{e}(\tau)d\tau \tag{5}$$

The first n – 1 terms of this series are easily approximated using the trapezoid rule. The final term requires additional consideration as $\hat{\sigma}(0)$ is undefined for many dispersions that are commonly studied in geophysical problems. These extra steps will not be derived here. See Marchant (2015) for a complete derivation.
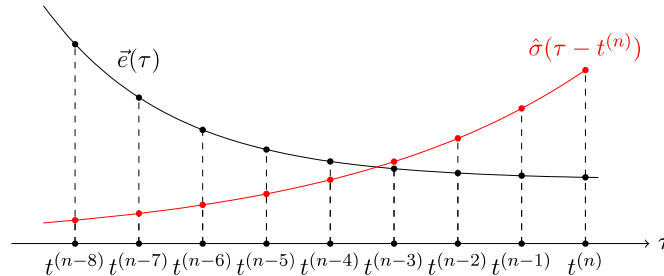
Figure 1 - Depiction of the terms involved in the evaluation of Equation (3)

Applying the trapezoid rule, and collecting like terms allows Equation **(5)** to be written simply as

$$\vec{j}(t) = (\sigma_{\infty} - \gamma(\delta(0t^n)))\vec{e}^{(n)} - \vec{j}_p^{(n-1)} \tag{6}$$

where
$$\vec{j}_p^{(n-1)} = \sum_{k=1}^{n-1} \frac{\delta t^{(k)}}{2}\left[\hat{\sigma}(t^{(n)} - t^{(k-1)})\vec{e}^{(k-1)} + \hat{\sigma}(t^{(n)} - t^{(k)})\vec{e}^{(k)}\right] + \kappa(\delta t^{(n)})\vec{e}^{(n-1)} \tag{7}$$

In these expressions, γ and κ are relationships derived from the asymptotic behaviour of the impulse response of the conductivity spectra.
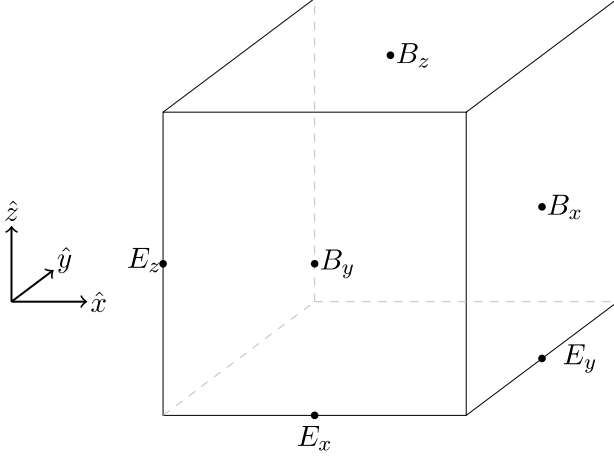
Figure 2 - Discretization of a cell. The electric field is placed on cell edges and the magnetic flux density is placed on cell faces. Physical properties are placed at cell centres.

Discretization of Maxwell's Equations

Applying a backward Euler discretization in time to Equation (3) results in

$$\vec{\nabla} \times \vec{e}^{(n+1)} + \frac{\vec{b}^{(n+1)} - \vec{b}^{(n)}}{\partial t^{(n+1)}} = 0$$
$$\vec{\nabla} \times \frac{1}{\mu}\vec{b}^{(n+1)} - \vec{j}^{(n+1)} = \vec{J}_s^{(n+1)} \tag{8}$$
$$\vec{j}(t) = (\sigma_\infty - \gamma(\delta(0t^n))\vec{e}^{(n)} - \vec{j}_p^{(n-1)}$$

The earth is now discretized onto an orthogonal tensor mesh where physical properties are located at cell centres, electric fields and current densities located on cell edges, and magnetic fields are located on cell faces. This discretization is shown in Figure 2. Let **b**, **e** and **j** be grid functions that are the staggered discretization of $\vec{b}$, $\vec{e}$ and $\vec{j}$. Using a standard staggered discretization of the differential operators, the following system of discretized differential equations is obtained

$$Ce^{(n+1)} + \frac{b^{(n+1)} - b^{(n)}}{\delta t^{(n+1)}} = 0$$
$$C^T M_{\mu^{-1}}^f b^{(n+1)} - M^e j^{(n+1)} = M^e j_s^{(n+1)} \tag{9}$$
$$M^e j^{(n+1)} = M_A^e e^{(n+1)} - j_p^{(n)}$$

In these equations, C and C^T are are the discrete curl operators which map from edges to faces or faces to edges, respectively. The vector j_p is a discrete representation of $\vec{j}_p$, given by

$$j_p^{(n)} = \sum_{k=1}^{n} \frac{\delta t^{(k)}}{2}\left[M_{\hat{\sigma}(n,k-1)}^e e^{(k+1)} + M_{\hat{\sigma}(n,k)}^e e^{(k)}\right] + M_\kappa^e e^{(n)} \tag{10}$$

The matrices M are mass matrices which map the property denoted by the subscript from cell centres to the location denoted by the superscript (faces or edges).

Combining the equations in **(9)** results in a linear system relating the magnetic fields at the time $t^{(n+1)}$ to the magnetic fields and current densities at time $t^{(n)}$

$$\left(M_{\mu^{-1}}^f C M_A^{e^{-1}} C^T M_{\mu^{-1}}^f + \frac{1}{\partial t^{(n+1)}} M_{\mu^{-1}}^f\right) b^{(n+1)} = \frac{1}{\partial t^{(n+1)}} M_{\mu^{-1}}^f b^{(n)}$$
$$-M_{\mu^{-1}}^f C M_A^{e^{-1}} j_p^{(n)} + M_{\mu^{-1}}^f C M_A^{e^{-1}} M^e j_s^{(n+1)} \tag{11}$$

Given the fields at previous time steps, Equation **(11)** is solved for the magnetic fields at $t^{(n+1)}$ and Equations **(9)** and **(10)** are then used to calculate the electric fields and current densities.

RESULTS

Validation

To test the implementation of the convolution-based forward modelling, the step-off responses of a vertical magnetic dipole source located at the surface was simulated. The simulations were performed for various uniform half-space models, and the results were compared to the results obtained from transforming frequency domain analytic expression for the same survey geometry.

For the tests, the earth was discretized onto a cylindrical mesh. The core region or the cylindrical mesh was comprised of twenty-five 2.5 m cells in the radial direction, and twelve, 2.5 m cells in the vertical direction. The core region was padded with an additional thirty-five cells in the up, down and radial directions. The padding cells were expanded with a fixed ratio of 1 to 3. The time axis was discretized into 400 segments, with 100 steps taken with each of four values of $\delta t = (10^{-5}s, 5 \times 10^{-5}s, 2.5 \times 10^{-4}s$ and $1.25 \times 10^{-3}s.)$

The receiver was placed 50 m from the transmitter which had a dipole moment of $1 Am^2$. Both the transmitter and the receiver were located on the surface of a uniform chargeable half-space. The half-space had Cole-Cole parameters of $\sigma_\infty = 10^{-2} S/m$, $\eta = 0.75$ and $\tau = 1s$. Simulations were run for four values of c=(1.0, 0.75, 0.5 and 0.25).

(a) c = 1.00

(b) c = 0.75

(c) c = 0.50

(d) c = 0.25
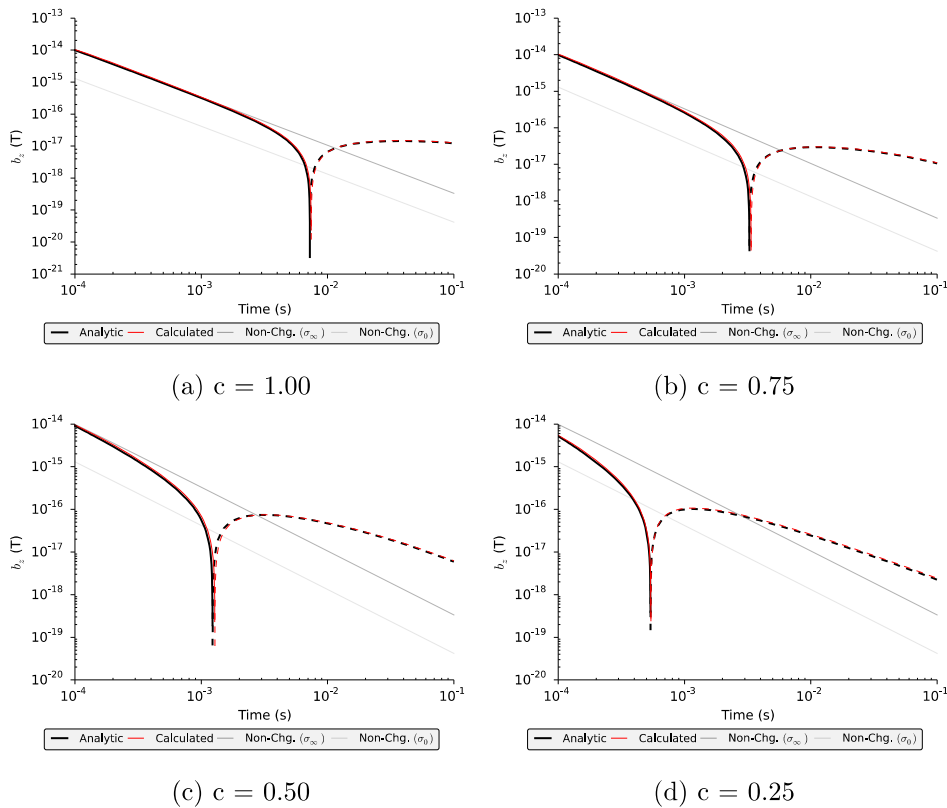
Figure 3 - A comparison of the magnetic fields simulated using the convolution algorithm and the transformed analytic expression. Excellent agreement between the pair of decays is obtained for all examples.

Three-Dimensional Example

(a) Debye dispersion ($c = 1$)

(b)
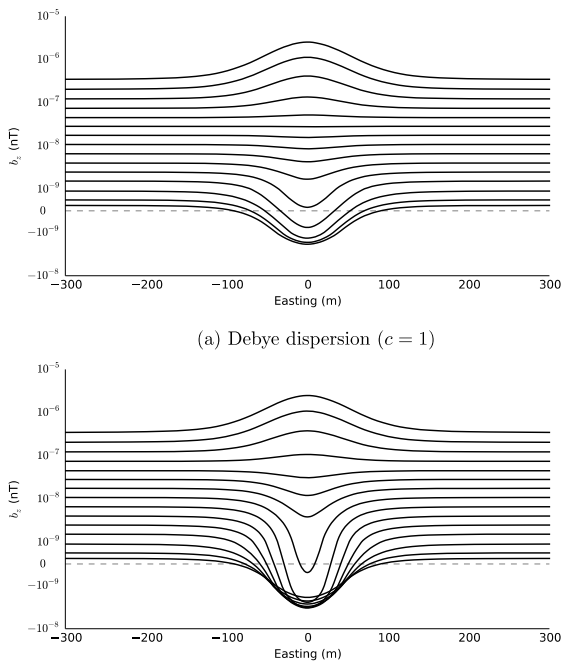
Figure 4 - Bi-log plot of the vertical component of the calculated b-field data for a block exhibiting Debye dispersion (a) and a Warberg dispersion (b).

The convolution method will now be demonstrated on a synthetic three-dimensional example. The physical property model for this test consists of a chargeable block placed in a uniform, non-chargeable background. The block has dimensions 100m×100m×80m with the top of the block 40m below the surface. The block has Cole-Cole parameters of $\sigma_\infty = 10^{-1} S/m$, $\eta = 0.3$ and $\tau = 0.1s$. Simulations were performed for two different values of c, a Debye model with c = 1, and a Cole-Cole model with c = 0.5. The background has a conductivity of $10^{-3} S/m$.

Vertical point dipole transmitters with unit dipole moments are placed in a single line passing directly over the centre of the block at 30m intervals, 30m above the surface of the model. Receivers are modelled to be co-located with the transmitters, measuring the vertical component of the magnetic field.

The conductivity model is discretized onto a regular tensor mesh with core cells of 20m on a side. The core region consists of $31 \times 11 \times 20$ cells. 15 padding cells, growing by 30% with each cell, are then added in each direction. This results in a $61 \times 41 \times 50$ cell mesh (125050 cells in total) modelling a 9.3km × 8.9km × 9.1km volume. Time is discretized into 160 steps, using four values of δt (1 × 10−5, 5 × 10−5, 2.5 × 10−4 and 1.25 × 10−3s) and 40 steps being taken for each value.

The resulting b-field data is shown in Figures 4 and 5. Figure 4 shows the b-field response along the line as a bi-log plot. In this

figure, each line represents the magnitude of the magnetic field at a single time channel. The plotted lines represent 15 different times logarithmically distributed between 10^{-4}s and 10^{-2}s. On a bi-log plot, both positive and negative values are plotted logarithmically, with the transition zone (in this case between $\pm10^{-9}$nT) plotted linearly. Figure 5 shows the decay of the magnetic fields recorded directly over the centre of the chargeable block for both values of c, as well as the decay of the non-chargeable σ_∞ model. The y-component of the computed current densities at a few times is shown in Figure 6.

Figure 5 - Time decay of the magnetic field for Debye (Black), Warberg (Red), and non-chargeable (Gray) 3D models. Plotted decays come from the transmitter receiver pair located directly over the centre of the chargeable block. Negative values are shown as dashed lines.
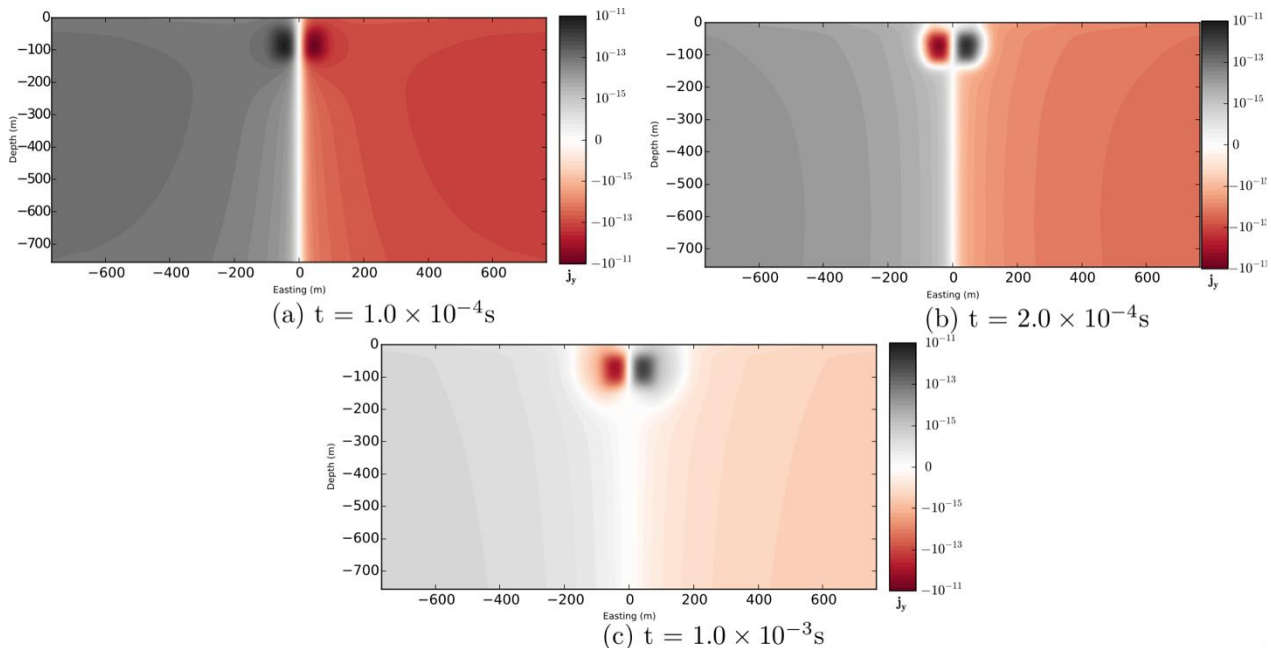
Figure 2 - The y-component of current densities produced from the transmitter located at x=0m and z=30m and the c=0.5 model. (a) Initially, a strong positive response is observed in the block and the background. (b) At later times, the direction of current flow has reversed in the block. Even though the direction of current flow in the block has reversed and is decaying back to zero, the decay of the remaining positive background response still dominates. (c) At late times the response at the receiver is negative, resulting from the decay of the polarization currents in the block.

CONCLUSIONS

In this work, a new technique for modelling time domain electromagnetic experiments in the presence of chargeable materials was presented. This technique works directly in the time domain by numerically approximating the convolution that appears when transforming Ohm's law for frequency dependent conductivities back to the time domain. The resulting method eliminates the need of Fourier transforms and only requires the solution of real, symmetric, positive definite systems rather than complex, non-Hermitian systems that are present in frequency-domain modelling.

Modelling tools can be used to provide a better understanding of observations of IP effects in TEM data. For example, a suite of simulations for varying physical property distributions could provide an understanding of the extent or physical property range that gives rise to observations of negative transients in central loop survey data. These methods can also be used to provide a better understanding of the manifestation of IP effects in non-centre loop TEM survey designs. The simulated results could also be used to test new ideas on how to recognize or interpret IP effects.

REFERENCES

Bhattacharyya, B. (1964). Electromagnetic fields of a small loop antenna on the surface of a polarizable medium. Geophysics, 29(5):814–831.

Commer, M., Petrov, P. V., and Newman, G. A., (2017). FDTD modelling of induced polarization phenomena in transient electromagnetics. Geophysical Journal International, 209(1):387–405

da Silva, N. V., Morgan, J. V., MacGregor, L., and Warner, M. (2012). A finite element multi-frontal method for 3D CSEM modelling in the frequency domain. Geophysics, 77(2):E101–E115.

Flis, M., Newman, G. A., and Hohmann, G. W. (1989). Induced- polarization effects in time-domain electromagnetic measurements. Geo- physics, 54(4):514–523.

Hohmann, G. W. and Newman, G. A. (1990). Transient electromagnetic responses of surficial, polarizable patches. Geophysics, 55(8):1098–1100.

Lee, T. J. (1975). Sign Reversals in the Transient Method of Electrical Prospecting (OneLoop Version). Geophysical Prospecting, 23(4):653–662.

Lee, T. J. (1981). Transient electromagnetic response of a polarizable ground. Geophysics, 46(7):1037–1041.

Lee, T. J. and Thomas, L. (1992). The Transient Electromagnetic Response of a Polarizable Sphere in a Conducting Half Space. Geophysical prospecting, 40:541–563.

Lewis, R. J. G. and Lee, T. J. (1984). The Detection of Induced Polarization with a Transient Electromagnetic System. IEEE Transactions on Geoscience and Remote Sensing, GE-22(1):69–80.

Marchant, D., Haber, E., and Oldenburg, D. W. (2014). Three-dimensional modelling of IP effects in time-domain electromagnetic data. Geophysics, 79(6):E303–E314.

Marchant, D., 2015, Induced Polarization Effects in Inductive Source Electromagnetic Data: Ph.D. Thesis, University of British Columbia

Morrison, H. F., Phillips, R., and O'Brien, D. (1969). Quantitative interpretation of transient electromagnetic fields over a layered half space. Geophysical prospecting, 14:82–101.

Newman, G. A., Hohmann, G. W., and Anderson, W. L. (1986). Transient electromagnetic response of a three-dimensional body in a layered earth. Geophysics, 51(8):1608–1627.

Rathor, B. (1978). Transient electromagnetic field of a polarizable half-space due to various current pulses. Geophysical Prospecting, 26:337–351.

Smith, R. S., Walker, P., Polzer, B., and West, G. F. (1988). The time-domain electromagnetic response of polarizable bodies: an approximate convolution algorithm. Geophysical Prospecting, 36(April):772–785.

Streich, R. (2009). 3D finite-difference frequency-domain modelling of controlled-source electromagnetic data: Direct solution and optimization for high accuracy. Geophysics, 74(5):F95–F105.

Wait, J. and Debroux, P. (1984). Induced Polarization in Electromagnetic Inductive Schemes. Geophysical prospecting, 32:1147–1154.

Zaslavsky, M. and Druskin, V. (2010). Solution of time-convolutionary Maxwells equations using parameter-dependent Krylov subspace reduction. Journal of Computational Physics, 229(12):4831–4839.

Zaslavsky, M., Druskin, V., and Knizhnerman, L. (2011). Solution of 3D time-domain electromagnetic problems using optimal subspace projection. Geophysics, 76(6):F339–F351.